

Localization and Conversion of Single Cell Positions from Static High-Resolution Digital Images to Lasermicrodissector Coordinate System through Utilization of References and 2D Transformation Techniques

Marianna Dimitrova Kucarov¹, Béla Molnár², and Miklos Kozlovsky³

¹Doctoral School of Applied Informatics and Applied Mathematics, BioTech, Óbuda University, 3DHistech Ltd., Budapest, Hungary, kucarov.marianna@uni-obuda.hu

²3DHistech Ltd., Budapest, Hungary, bela.molnar@3dhistech.com

³John von Neumann Faculty of Informatics, Óbuda University, Bécsi Str. 96/b, 1034 Budapest, Hungary, kozlovsky.miklos@nik.uni-obuda.hu

³Medical Device Research Group, LPDS, Institute for Computer Science and Control (SZTAKI), Hungarian Research Network (HUN-REN), Kende Str. 13-17., 1111 Budapest, Hungary, kozlovsky.miklos@sztaki.hu

Abstract: A laser microdissection technique for tissue excision has been developed to replace the slow, manual positioning of the laser with a roller. The method consists of the 3DHistech-P1000 digital tissue scanner, MorphCheck evaluation software, and integration of the MMI CellCut laser microdissector. To create a seamless integration between the workflows, a digital reference selection; rotational, translational, and conversion transformation of Region of Interest (ROI) coordinates from pixel-based images to the mm-based coordinate system of the laser unit; a fused database loaded with parameters (image, shape, position, unique identifier) of the analyzed slides and the selected ROIs, and XML-based communication have been developed. The software implementation has been tested on the microdissector device. The application of the method results in an automated workflow that allows laser excision with an accuracy of 2 μm and a standard deviation of 2.2 μm , which requires the selection of at least three cell clusters of ROIs to perform laser excision without live image based on a predefined static image.¹

Keywords: digital tissue scanner; MorphCheck; laser capture microdissection (LCM); pathology workflow automation; automatic tissue dissection

¹ The authors gratefully acknowledge the financial support of the 2019-1.3.1-KK-2019-00007 "Establishment of an innovation service base for the development of cyber-medical systems for diagnostics, therapeutics and research" project financed by the National Research, Development and Innovation (NRDI) Office Hungary.

1 Introduction

Tissue microdissection has emerged as a pivotal technique used in molecular biology and pathology to isolate specific cells or regions of interest from tissue samples. The goal is to obtain pure populations of cells for various downstream analyses [?], such as genomic [1], transcriptomic [2], proteomic [3], [4], or epigenomic [5] studies. This technique is particularly valuable when studying heterogeneous tissues where different cell types coexist.

Over the years, the field has witnessed the evolution of tissue microdissection techniques [6], [7] from manual to semi-automatic microdissection types [8]. Manual microdissection technique involves manually dissecting or isolating specific cells or regions using fine needles, blades, or other microtools. During the procedure, tissue sections are often stained to enhance the visibility of specific structures or cell types [9]. A trained researcher visually identifies and collects target cells or regions using a micromanipulator or other precision instruments under a microscope. This process demands a high level of expertise and precision, as the goal is to dissect cells without compromising their integrity. Manual microdissection offers advantages such as a low equipment cost and versatility in application across a wide range of tissues. However, the technique is characterized by its time-consuming and labor-intensive nature. Moreover, there is a higher risk of contamination compared to other methodologies. Additionally, manual microdissection exhibits limited precision in comparison to more advanced techniques like LCM. Key suppliers of tools and instruments tailored for manual microdissection include World Precision Instruments (WPI), Ted Pella, Inc., Sutter Instrument Company, Fine Science Tools (FST), and Roboz Surgical Instrument Co.

Meanwhile, one of the most commonly used semi-automatic procedure is laser cutting. The general operation of Laser Capture Microdissection (LCM) is presented in Figure 1. It utilizes a laser beam and adhesive capsule to precisely cut and capture specific cells or regions of interest [10]. The tissue section is typically mounted on specialized membrane microscope slides for the procedure. A laser is directed through the microscope lens and the slide by a computerized system [11]. The user identifies and marks the target cells or regions on a computer screen. The laser then precisely cuts and captures the selected material, which is collected for example in Eppendorf tubes for subsequent analysis [12]. The advantages of LCM include high precision, spatial resolution, and minimal contamination, rendering it suitable for downstream molecular analyses [9]. However, the technique comes with some drawbacks, including a higher equipment cost, complex instrumentation, and the potential for sample damage due to laser exposure. Laser dissection can be performed by Molecular Machines & Industries (CellCut, CellEctor [13]), Leica Microsystems (LMD6500, LMD7000 [14]) and ThermoFisher Scientific (Arcturus LCM [15]) companies. Besides laser cutting, Instrumedics Inc. (CryoJane Tape-Transfer Sys-

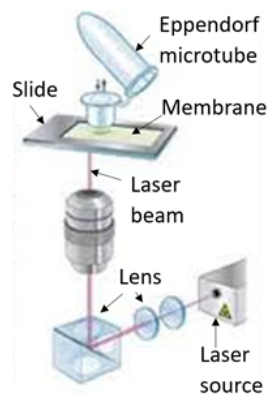


Figure 1
Operation of laser capture
microdissection

tem [16]) and Leica Biosystem (Cryostat CM3050 S [17]) carry out tissue excision with liquid nitrogen. Medtronic (Valleylab FT10 Energy Platform [18]) and Olympus (SurgMaster electrosurgical system, Thunderbeat [19]) dissect with electric current (electrocauterization). Chemical solvent-based procedures are used by Sigma-Aldrich (Merck KGaA) and Thermo Fisher Scientific (Histological Reagents), while Worthington Biochemical Corporation and Roche Applied Science (Liberase TM Research Grade enzyme blend [20]) are capable of tissue excision with enzymes. Furthermore, frozen tissue is dissected by Sakura Finetek (Cryostat Tissue-Tek [21]) and Leica Microsystems (Cryo-Ultramicrotomes System [22]).

While both manual microdissection and LCM provide a stable basis for tissue microdissection [23], there is an ongoing pursuit of improvement in several aspects [24]. The microdissection process requires technical experts in handling tissues and microdissection tools. It is still time-consuming, and there is a risk of sample integrity, contamination, or degradation during and between the scanning and laser-cutting process.

In the course of our research so far on the smooth connection of pathology workflow, we have found that there are still ineliminable parameters with uncertainties during tissue preparation, slide scanning as well as laser dissection, due to hardware and software limitations [25]. For example, in a tissue scanner, there is a frame that holds the slide in the scanner stage, but unfortunately, it obscures the upper part of the whole slide, hence the origin of the absolute coordinate system is missing. Another uncertainty is that there is some leeway in the scanner stage holder in order to have enough space to insert different slides into the stage. Resulting the fact that a changing amount from the upper part of the slide is missing from the digital images. Also, stitching uses best-fit algorithm to merge tiles together. It means there is some randomization during image creation. Hence, it cannot be eliminated using calibration. Moreover, the LCM stage has leeway similarly to the scanner mentioned before. These findings suggest the need to include references to link the equipment. The references should be placed only on the slides since this is the only component that passes through each piece of equipment.

In light of the existing literature, specific questions arise regarding the possible link between the tissue scanner and the dissector. None of the above-mentioned dissection procedures on the market is coupled with a high-resolution and high-performance digital tissue scanner, such as the 3DHistech P1000 tissue scanner. They are only assembled with a digital microscope, which shows a live image with a small field of view. Thus, it is still necessary to manually scan the sample by eye through the small field of view, focus each time, select the ROIs one by one, position the stage with a joystick so that the tissue to be excised is above the laser beam, and then cut the ROIs. Thus the aim is to automate and speed up these manual steps so that, a pre-scanned static image could be used to evaluate and pre-select which areas should be excised taking into account the entire sample, and then excise them all in sequence. The feasibility of establishing this link is a primary concern, which requires a detailed exploration of the associated methods. An essential aspect is the identification and formulation of possible limitations to such integration. Furthermore, in the context of automating the workflow, the evaluation of the maximum

achievable excision accuracy becomes an important issue. Clarifying the answers to these questions is the primary objective of this paper, which is organized as follows.

Section 2.1 presents the experienced physical reference marking techniques during membrane slide preparation. Section 2.2 briefly describes the subsequent digital slide scanning details. Section 2.3 explains the main steps of MorphCheck software development, such as digital reference marking built on Section 2.1, tissue sampling, digital storage creation and insertion for sampling as well as XML communication with laser microdissector. Section 2.4 focuses on the LCM operation settings, slide viewer handling, application of the developed MorphCheck features, and the automatic region of interest (ROI) transfer to real-time images. In Section 3, the implementation and the integration of the software-hardware design are tested, and the results are gathered, compared, and analyzed. In the last section, results are summarised, a conclusion is made and the potential next phase steps and the future direction of research are discussed, too.

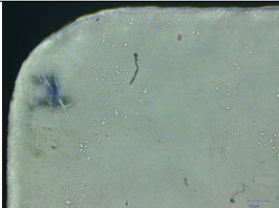
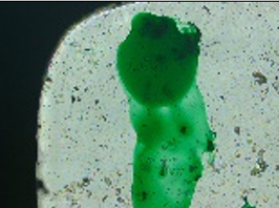

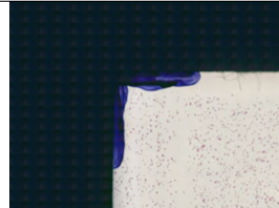
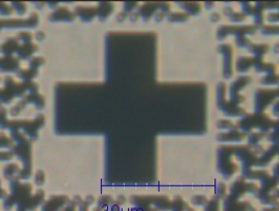
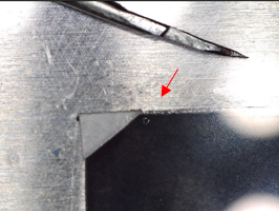



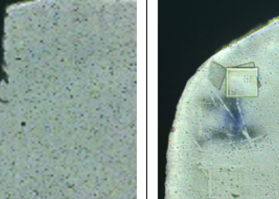
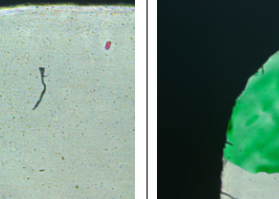
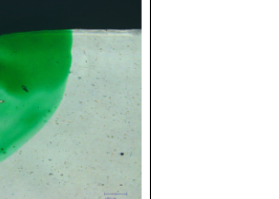
2 Materials and Methods

2.1 Reference marking on slides

The use of a reference is essential to establish a transformation between two coordinate systems. The scanner and the dissector device operate independently, it is only the slide that interacts with both machines. Since this is the only object that is common, it is necessary to create the reference points on the slide in a way that is usable by both devices. Table 1 gathers the experimented reference marking techniques applied at the four inner corners of membrane slides with metal frames during tissue preparation. The following strategies were tried:

1. No reference/Marking by eyes
2. Alcohol felt-tip pen marking:
 - 2.1. Dot shape
 - 2.2. Cross shape
 - 2.3. Corner shape
3. Test slide with its own printed crosses used as reference
4. Hole punching with a medical scalpel
5. Marking with stickers:
 - 5.1. Cross shape
 - 5.2. Triangle shape
 - 5.3. Square shape
6. Laser cut references:
 - 6.1. Cut square shape
 - 6.2. Cut cross shape

Table 1
 Tried reference types in the upper left corner of membrane slides

1. no marker usage	2.1 Alcohol felt-tip pen marking – dot shape	2.2 Alcohol felt-tip pen marking – cross shape	2.3 Alcohol felt-tip pen marking – corner shape
			
3. Printed cross reference	4. Hole punching	5.1 Marking with stickers – cross shape	5.2 Marking with stickers – triangle shape
			
	5.3 Marking with stickers – square shape	6.1 Laser cutting reference – cut square shape	6.2 Laser cutting reference – cut cross shape
			

2.2 Tissue scanning before laser cutting

For scanning, the **PANNORAMIC 1000** equipment manufactured by 3DHistech was used. It is the largest-capacity whole-slide tissue scanner on the market with 1000 slides. Its magazine panels support Leica and Sakura slide racks, compatible with several stainer-coverslippers. Optional water immersion with a precision pipetting unit and water quantity sensor, multilayer (Z-stack) and extended focus scanning are available. Intensity stitching with compensation works also on the Z axis. Slide loading and scanning are fully automatic enabling unsupervised operation for whole day's needs.

The operation of the P1000 scanner can be found in its attached user guide [26]. The settings about focus, color balancing, scanning mode, magnification, immersion type, multilayer mode, and stitching were saved in a profile for reusability during scanning. In total 36 slides were scanned, of which 9 pieces (1.-9.) were scanned without any markers, as they are currently scanned in industry for comparison reasons. 9 slides were marked using an alcohol felt-tip pen, of which 7 pieces (10.-16.) had a dot shape, 1 slide (17.) had a cross shape and another one (18.) had a corner shape marker. 1 membrane (19.) was hole-punched with a medical scalpel. 5 slides have been stickered, of which 1 (20.) got a cross shape, 2 slides (21-22.) got triangle shape and another 2 pieces (23-24.) got square shape stickers. 11 slides got laser-cut marker, of which 6 pieces (25.-30.) had square shape and 5 (31.-35.) had cross shape excision. In addition, a tester slide (originally for calibration purposes) (36.) were included in the experiment where its own printed crosses were used as reference. The files of scanned membrane slides could not be attached to the journal due to their large size, but can be requested from the authors. Their scanning results, quality, and therefore their possible usage are collected in the Results section.

2.3 MorphCheck development

The tissue scanning was followed by the evaluation of the digital images using **MorphCheck** software. It is capable of opening images digitized by a tissue scanner and checking at a basic level whether they can be evaluated. It supports the special data storage format used by 3DHistech scanners as well as simple digitized tissue images. It can handle commonly used staining methods: H&E (Hematoxylin-Eosin), DAB (3,3'-Diaminobenzidine), and multicolor fluorescence staining. It works by identifying individual tissue components based on their fractal parameters. The operation of the MorphCheck software can be found in its attached user guide [27]. New features such as digital reference marking, metadata generation and calculation during tissue sampling, automatic data saving into PostgreSQL database, and communication with LCM have been developed and tested, which are also part of the main technical contributions of the current paper.

2.3.1 Reference marking in MorphCheck

After opening a 3DHistech slide in MorphCheck, a scan map of the whole slide displays on the left side of the view, while a zoomed subpart image at the marker position appears on the right side of the view together with a new activated reference selection \oplus button presented in Figure 2. Reference points have to be selected and

saved before the ROIs so that the relative positions of the ROIs can be calculated. It is worth noting the order of the reference selection as it has to be repeated later in LCM for the actual position transfer of the ROIs. A laser cut cross reference marking is shown in Figure 2.

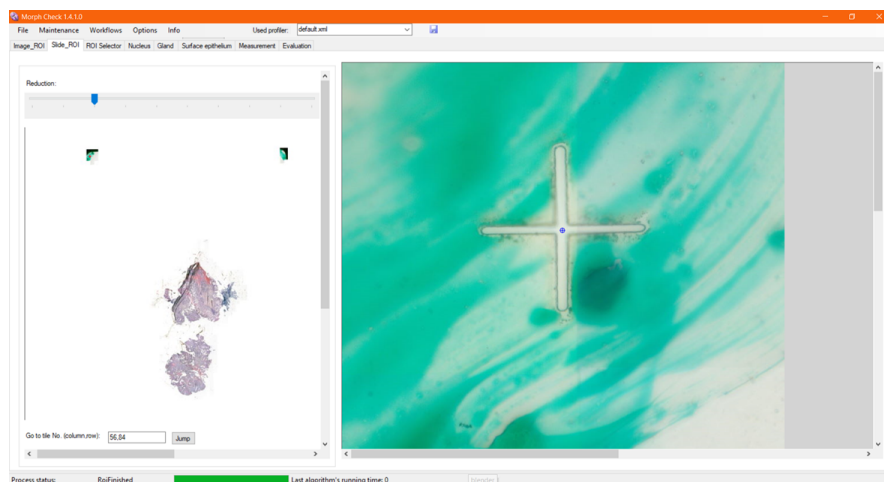




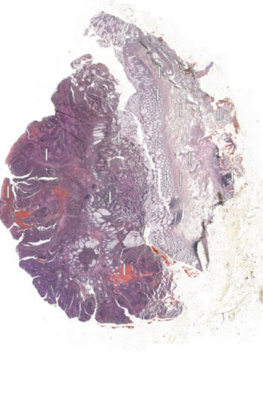
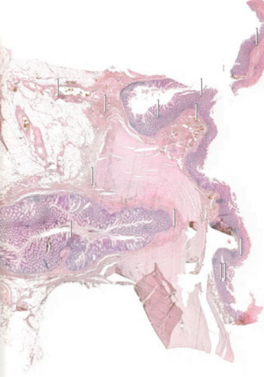

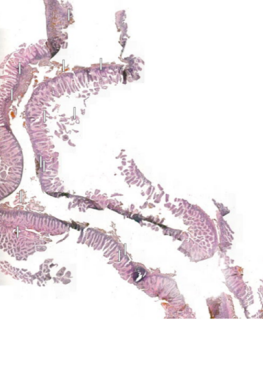



Figure 2
Reference marking of the cut cross shape marker in MorphCheck

2.3.2 Tissue sampling, ROI selections

After the reference points are fixed, the region of interest can be selected [28]. Table 2 presents six examples of membrane slides being examined with a total of 283 ROI selections for genomic analysis. As a ROI is being saved a new roll-down window pops up at its location (above its frame) shown in the slides of Table 2. In the background, the following metadata is calculated that is displayed in the roll-down windows:

- ID of the ROI, generated by MorphCheck
- ID of the used slide, generated by the tissue scanner
- Shape of the ROI
- Zoom level where ROI is selected.
- Relative position of the ROI in pixel according to image magnification set
- Absolute position of the ROI in pixel which is the bottom layer of the image pyramid (zoom level=0)
- Absolute position that is transformed from pixel-based coordinate system to mm based coordinate system of the dissector

Table 2
Number and position of the selected ROIs in slides (samples)

<p>TestSlide – 150 pieces of ROI</p> 	<p>C.J – 4 pieces of ROI</p> 	<p>M 1 – 18 pieces of ROI</p> 
<p>William 1 – 12 pieces of ROI</p> 	<p>William 2 – 12 pieces of ROI</p> 	<p>William 3 – 13 pieces of ROI</p> 
<p>12418 19 N+K B-2 – 13 pieces of ROI</p> 	<p>14111 31 – 12 pieces of ROI</p> 	<p>M 2 – 16 pieces of ROI</p> 

2.3.3 Storage of tissue sampling

Morphology and genomics fused database architecture was designed and created in a previous development phase [29]. Currently, its automatic data insertion during ROI selection on MorphCheck GUI has been implemented using asynchronous operation for time efficiency. The parameters of SLIDE, ROI tables such as field names, data types and their constraints can be seen in Attachments/Figure 9 and 10. They also contain the uploaded slides being examined and the selected ROIs during tissue sampling.

2.3.4 Communicaton between MorphCheck and the microdissector

A, Xml file creation

Communication between the MorphCheck software and the LMC could be obtained via XML files. An XML file is automatically generated in the background during ROI sampling in the GUI [25]. It expands with the calculated metadata parameters of the new ROIs being saved. The forwarded parameters are listed in Section 2.3.2. An example XML file is shown in Attachments/Figure 11, the middle of which contains all the selected ROI shapes and their necessary properties for laser cutting.

B, Dissector calibration

Under normal circumstances, the calibration of the slide holder stage remains valid unless the stage is moved manually or using software other than MMI CellTools. If the software detects an invalid stage calibration, slide scanning will be disabled. In this case, to recalibrate the stage, start the calibration procedure by one of the following options:

- Press the Calibrate origin  icon in the Slide Viewer.
- Setup → Click on Calibrate Stage origin button.

During the calibration process, the microscope objective will move down and the stage will move to its limit switches. If the stage geometry is still not matching a scanned overview image, the stage geometry configuration needs to be adjusted, described in Section 2.4.2. The calibrated coordinate-system parameters then can be exported to an XML file shown in the upper part of Attachments/Figure 11. The XML was forwarded to MorphCheck which uses the stage geometry during the position transformation of the ROIs. If the coordinate system changes again, then a new calibration results has to be send to MorpCheck for updating.

C, Template generation for reference points

An XML template has been created for the cross-shaped, laser-cut references that can be used for any membrane slide being examined before tissue scanning. The template has to be imported to LCM and start the laser-cut. During the process, the 4 cross shapes at the corners of the membrane are cut out. The cutting is done in the order of upper left, bottom left, bottom right and then upper right corner. The references produced can be found in the last part of Attachments/Figure 11.

D, Export from MorphCheck

A new „Export ROIs” feature has been developed in the MorphCheck GUI to get the desired XML file. (Latter can be found in the Attachments.) Thus, the file can be saved to the local PC and forwarded to the LCM.

2.4 Operating the laser microdissector

The MMI CellCut equipment was applied as LCM which is manufactured by Molecular Machines & Industries. It facilitates precise and contamination-free laser dissection of cell clusters, single cells, or subcellular compartments from various types of tissues including fresh frozen, paraffin-embedded and archived slides, cytopins, smears, and even living cells.

2.4.1 Settings

The MMI CellCut is a complex system that requires the following steps to be executed in order to start its operation [30]:

1. The PC has to be started and the boot process must be completed first.
2. The white light power supply of the microscope shown in Figure 9/a should be turned on.
3. The fluorescent light power supply of the microscope presented in Figure 9/b needs to be turned on.
4. The CellCut controller should be switched on by turning the key as illustrated in Figure 9/c.
5. The laser should be powered on by pressing the button on the CellCut controller. Thus the LED turns orange at the laser status sign.
6. The Olympus controller shown in Figure 9/d should be powered on with the switch on the back. Start its operation.
7. The slide(s) should be prepared, with the tissue mounted on the flat side of the membrane slide. After that, the membrane with the tissue should be inverted upside-down and placed onto a support glass slide. Thus the tissue is now under the membrane and over the glass slide, thereby making a „membrane-tissue-glass slide” sandwich shown in Figure 9/e. This way, the tissue is protected against contamination.
8. The prepared slide should be placed in the microscope stage.
9. An Eppendorf microtube should be inserted into the cap lift component.
10. The MMI CellTools software needs to be started, and one should wait until the software has finished the start-up and self-test procedure. The currently installed software version is 5.1.3.
11. The 40x objective should be selected at the CellTools GUI and also on the Olympus controller. It switches the objective into the path of the light inside the microscope.
12. A preview should be made from the slide.
 - 12.1. If the function is disabled then stage origin has to be calibrated as described in Section 2.3.4.
 - 12.2. If the preview result does not precisely cover the desired slide area then the stage has to be configured in accordance with Section 2.4.2.
13. Finally, the laser parameters need to be set, detailed in Section 2.4.6.

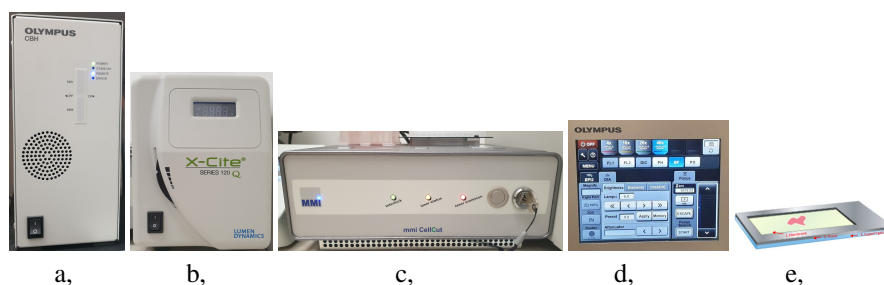











Figure 9

a, White light power supply; b, Fluorescent power supply; c, CellCut controller; d, Olympus control box; e, Membrane-tissue-glass slide “sandwich”

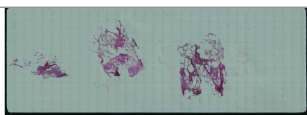
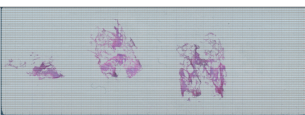
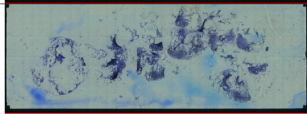
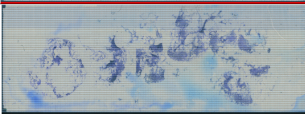
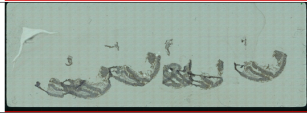

2.4.2 Slide Viewer & Previewing

Once the stage origin of the dissector is properly calibrated, preview image creation about the slide that is being inserted in the stage is enabled. To set previewing:

1. The desired microscope objective should be selected in the GUI and also in the Olympus control box. This action switches the right objective in the path of the light inside the inverse microscope.
2. The Slide Viewer should be opened by clicking on Settings  icon in the Slide scan and navigation panel, followed by configuring stage insert. Upon doing so, the Viewer window will appear, where the stage geometry is configured as outlined below:
 - 2.1. MMI membrane slide is selected as slide type in the Configure panel.
 - 2.2. The slides are moved in the viewer to their accurate position on the stage with the arrows , , ,  in the Shift panel. This feature facilitates the accurate alignment of a scanned overview image with the displayed slide. By the slide shifting procedure, the stage geometry can be corrected to precisely reflect the hardware.
 - 2.3. Subsequently, the active region being scanned has to be selected by the rectangle  drawing tool.
 - 2.4. Then settings can be saved and the Slide Viewer closed.
3. In Slide scan and navigation panel, preview scan should be started by clicking on the Start scan  button. If no area of interest was defined in the Slide Viewer, the maximal scan area will be used. The maximum scan area is the inner part of membrane slide. (Scanning process can be halted at any point with the Stop scan  button if deemed unnecessary.)
4. The created preview can be saved to disk by pressing the Save image  button. The file dialog enables the specification of the file name and image type (JPG, BMP, PNG, and TIF).



Previews in 10x and 40x resolution were made before transforming, and laser cutting. Three example pairs are shown in Table 3.

Table 3
Example preview samples with 10x and 40x objectives

Staining Type	10x objective	40x objective
H&E – on paraffin and frozen tissue, for cytoplasm, nucleus contrast ↓ CRC		
Gimza – on frozen tissue, for cytoplasm, nucleus contrast ↓ CRC		
DAPI – on paraffin and frozen tissue, for cytokeatin contrast if positive → native		

2.4.3 Import XML file into microdissector

The following steps describe the handling of an XML file.

1. The desired XML file - previously exported from MorphCheck in Section 2.3.4 - should be imported by clicking on the Import  icon in Groups panel shown in Figure 3. The imported shapes appear in the Groups panel.
2. By clicking on the group name, a window containing the list of ROIs pops up illustrated in Figure 4.
3. The Export  button needs to be pressed to save the areas in character-separated values (CSV) file, which can be opened by most data visualization and spreadsheet programs.
4. By a double click with the left mouse button on the area field in the shape list, the stage is navigated to the selected shape.

Of course, it is possible to load the previously created xml file again. However, it is not necessary to reload it for each annotation, as the xml loaded the first time contains all the annotations to be extracted for the given tissue sample. So after the xml import before the first cut, there is nothing further to do with it.

Into the bargain, the current laser dissector cannot detect that the tissue sample being excised and the xml are a pair, they match. However, the user can see the unique identifier of the tissue sample on the membrane slide. Furthermore, during the automatic generation of the xml file, its name is given based on



Figure 3
Group panel with the imported shapes





Figure 4
Shape list with area information for morphometry

the name of the opened digital tissue sample. This allows the user to verify whether the tissue sample has been inserted and the xml file has been imported into the user interface are name pairs or not.

2.4.4 Selecting reference points in the live field of view

Since the imported, predefined ROIs (Section 2.4.3) are unlikely to fall in the same place in the live image as they were exported in the static image, the marked reference points in the live image must be found to transform the ROIs to their accurate place. To do this, we utilize the serial section function of the machine. The Serial sections panel, shown in Figure 6, originally permits the dissection of the same objects on more than one slide. Objects can be marked on a master slide and subsequently copied to one or more section slides. However, we have used this feature on the same slide without jumping to a next slide for transformation purposes. In order to locate the objects on the section slides, a set of reference points (at least one and up to three) have to be provided. We have always used 3 references. The reference selections are outlined in the following steps:

5. A section layer is created in the Serial sections panel by activating the sections editor  icon.
6. A new layer is added like in Figure 5 then the editor can be closed.
7. The section layer for the active section is designated by clicking on the arrow. In the section layer, the reference points or ROIs are no longer visible in the Group panel.
8. The Create landmark tool  icon is pressed to mark the locations of the reference points.
9. The 3 reference points are identified in the live image, following the same order as they were laser cut in the membrane presented in Section 3.1, and selected in the static images explained in Section 2.3.1.
10. Upon completing the reference selection, they appear in the right side of the GUI by clicking the arrow next to the Create landmark icon, highlighted with red circle in Figure 6. Consequently, we have the reference points marked in the live field of view (section layer).

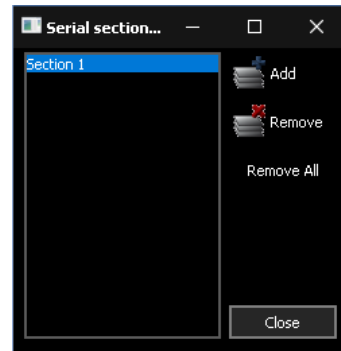


Figure 5
Serial section editor

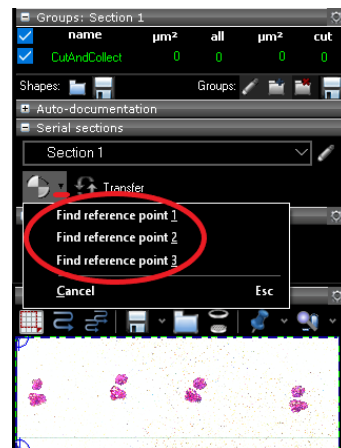


Figure 6
Serial Section panel, reference points marked in the section layer


Table 4
Transformation types with 1, 2, or 3 reference points [30]

Reference points	Types of transformation	Transformation preserves
1	translation	size, orientation and angles
2	translation, rotation and scaling	angles
3	translation, rotation, scaling and shearing	neither of the above

2.4.5 Transform ROI positions based on reference points

CellTools uses geometric transformations collected in Table 4 to map object positions and shapes. Reference points are used to define these transformations. For most applications, using at least two reference points is recommended. These should be clearly visible points in your section that are easy to locate precisely. Depending on the number of reference points used, CellTools will apply different types of changes to the original shape of the objects and thus accommodate variations in shape that were introduced in the sample preparation process. In our case, 3 reference points were being used that allowed translation, rotation, scaling, and shearing transformation as well.

The steps of the transformation are as follows:

11. Once the reference points have been located, the imported ROI points remain to be transferred from master to section layer. This can be done by pressing the Transfer  button next to Landmark tool icon, highlighted with red ellipse in Figure 7. All the shapes from the master layer are cloned to the section layer. The transformed ROIs appear in the Group panel of the section layer highlighted with red arrow in Figure 7.
12. If the group name is selected then then the window with the list of the transformed ROIs appear. The new ROI locations can be verified by clicking on their area values. Upon satisfaction, progression to Section 2.4.6 recommended. In the event of dissatisfaction, the transformation can be refined by relocating reference points more precisely in the section layer and subsequently activating the Transfer function again.

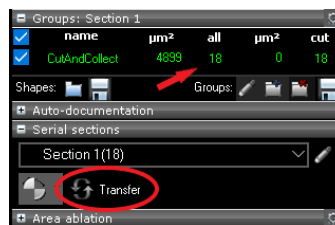



Figure 7
Transfer ROIs

2.4.6 Laser cutting ROIs

For optimal cutting performance, it is essential to properly adjust the laser properties for each objective and tissue type. In the Dissection panel, the following parameters were set empirically.

- Cut velocity = 30 $\mu\text{m}/\text{sec}$. The velocity slider defines how fast the stage moves during the cutting procedure itself.

- Laser focus = 553 μm . The focus slider adjusts the focus position of the laser beam in the z-direction within the tissue sample. The 0 mm position simply denotes that the laser focus position is as close to the objective as possible.
- Laser power = 88%. The power needed to cut the sample normally will be proportional to the sample thickness. Choose the power setting that enables clean laser cutting. Typical microscope objectives for fluorescence applications have UV transmissions between 80% and 95%. The actual laser power is not monitored in the device.
- Repeats = 2. In order to make sure the laser cut went through the whole tissue even where it is difficult to cut, e.g. very hard or thick tissue. The Repeat field indicates the number of times that the laser should process each shape.

If everything is set, the dissection of the ROIs can be initiated by activating the CutAndCollect  button. The results are shown in Figure 8.

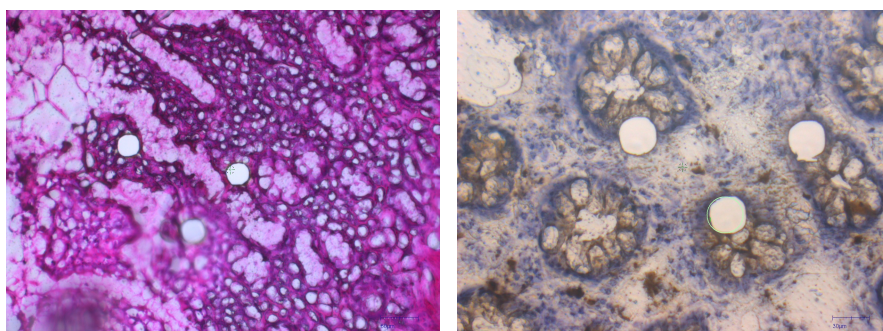


Figure 8
Laser cut tissue samples

3 Results and Discussion

3.1 Reference marking

Table 5 gathers the 36 scanned slides with 11 different markers, their preparation and resulting scan quality, their physical availability, and their potential use for further research. Without the use of a reference (1.-9.) - as is done today in the industry - it resulted in a maximum of 300 μm accuracy. The three different alcohol felt-tip pen markings (10.-16., 17., 18.) could not provide μm precision, although, the square-shaped one (18.) pointed out that angular reference is needed for higher accuracy. The tester slide (36.) with its own printed crosses used as reference had the accuracy of μm . It also proved that the smaller the reference the more accurate the results. However, is very expensive to produce, and therefore it is not attainable in routine clinics. The hole-punched marker with a medical needle (19.) and the stickers (20., 21.-22., 23.-24.) were not accurate enough. The latter did not withstand the physical movements or the chemical reactions. Meanwhile, both the laser-cut square (25-30.) and cross-shaped (31.-35.) markers were found to be suitable for mapping micro-

Table 5
Scanned slides and their properties

Slide ID	Properties	Physical slide availability	Usage
no references			
1 8808-04ep	old slide version, no physical slide available, no reference	-	test only
2 DigitalSlide_A6M_1S_1	old slide version, no physical slide available, no reference	-	test only
3 HT29_backflipped	not live tissue, backflipped, no reference	✓	test only
4 HT29_backflipped_II	not live tissue, backflipped, no reference	✓	test only
5 DW480	not live tissue, no reference	✓	test only
6 DW480_II	not live tissue, no reference	✓	test only
7 CaJ_CRC_16um	16 um is too thick	✓	test only
8 12418_19_N+K_B-2	good sample	✓	test only
9 14111_31	good sample	✓	test only
with references			
10 NAT_30_um_met_with_dot_ref_40x	cannot be scanned as 30 um is too thick, dot reference not accurate enough	✓	test only
11 K_CaJ_20um_with_dot_ref	20 um is still too thick, dot reference not accurate enough	✓	test only
12 CaJ_CRC_16um_blue_with_dot_ref	stood in Gimza staining too much --> contrast loss, 16 um is still too thick, dot reference not accurate enough	✓	test only
13 CaJ_CRC2_16um_with_dot_ref	16 um is still too thick, dot reference not accurate enough	✓	test only
14 12418_19_N+K_B-2_with_dot_ref_20x	dot reference not accurate enough, 20x	✓	test only
15 14111_31_with_dot_ref_20x	dot reference not accurate enough, 20x	✓	test only
16 TestSlide_with_dot_ref_40x	dot reference not accurate enough	✓	test only
17 HT29_backflipped_with_cross_ref_40x	cross reference not accurate enough	✓	test only
18 DW480_with_corner_ref_40x	corner reference not accurate enough	✓	test only
19 Hole_punched_ref_40x	Hole punched reference not accurate enough	✓	test only
20 CaJ_CRC_16um_with_cross_ref_40x	16 um is still too thick, cross reference not accurate enough	✓	test only
21 12418_19_N+K_B-2_with_triangle_ref_40x	thin enough, triangle reference not accurate enough	✓	test only
22 14111_31_with_triangle_ref_40x	thin enough, triangle reference not accurate enough	✓	test only
23 Kisfaludy_NAT_with_square_ref_40x	square reference not accurate enough	✓	test only
24 Kisfaludy_CRC_blue_with_square_ref_40x	square reference not accurate enough	✓	test only
25 12418_19_N+K_B-2_with_square_cut_ref_40x	thin enough, square cut reference accurate enough	✓	research
26 14111_31_with_square_cut_ref_40x	thin enough, square cut reference accurate enough	✓	research
27 Kisfaludy_CRC_blue_with_square_cut_ref_40x	thin enough, square cut reference accurate enough, membrane stretched during scanning, stood in Gimza staining too much --> contrast loss	✓	research
28 Kisfaludy_NAT_with_square_cut_ref_40x	thin enough, square cut reference accurate enough	✓	test only
31 Kisfaludy_NAT_with_square_cut_ref_40x_2	thin enough, square cut reference accurate enough, better scan than 1st time	✓	research
32 Kisfaludy_CRC_with_square_cut_ref_40x	thin enough, square cut reference accurate enough	✓	research
33 William_1_with_cross_cut_ref_40x	thin enough, cross cut reference accurate enough, cross reference is more intuitive	✓	research
29 William_2_with_cross_cut_ref_40x	thin enough, cross cut reference accurate enough, cross reference is more intuitive	✓	research
30 William_3_with_cross_cut_ref_40x	thin enough, cross cut reference accurate enough, cross reference is more intuitive	✓	research
34 M_1_with_cross_cut_ref_40x	thin enough, cross cut reference accurate enough, cross reference is more intuitive	✓	research
35 M_2_with_cross_cut_ref_40x	thin enough, cross cut reference accurate enough, cross reference is more intuitive	✓	research
36 TestSlide_with_its_cross_ref_40x	good, used its own pattern as reference	-	research

meter-precision transformations between independent devices that are feasible on slides and are inert from tissue sample processing. Additionally, cross-shaped markers proved to be more intuitive than cut square reference. Thereby, an XML template has been generated for the laser-cut cross references. Based on the above, the slides with IDs 25.-30., 31.-35., 36. slides were approved for further transformation evaluations.

3.2 Transformed ROIs





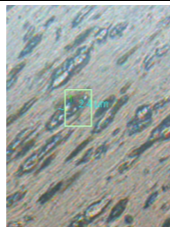

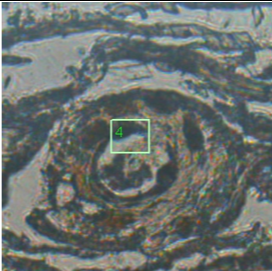
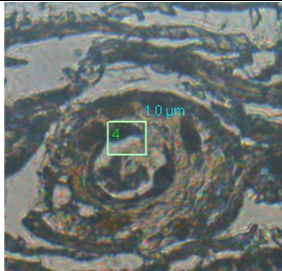
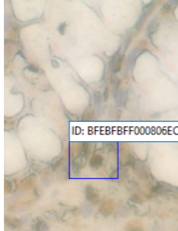
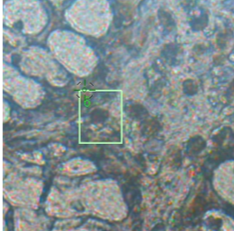
Images were saved about the location of transformed ROIs in LCM (Video → Save Image ). This allows their visual comparison with the areas selected in MorphCheck. Three examples are shown in Table 6. Distance between the target and the transferred position was also measured by using the measurement  tool, presented in the third column of the table.

Table 6
Transformed ROIs of M_2__with_cross_cut_ref_40x slide (samples)

ROI ID	MorphCheck ROI selection	Transformed ROI coordinate	Difference measuring
1			
4			
6			0 um

3.3 Evaluation of Results

The evaluation of the technique was made by the comparison of target and transferred positions based on parameters below:

- Target and transferred position: They were determined by placing laser position icon over the middle of the target and transferred shapes to read the mm-based position values of the laser icon in the left-bottom corner of the status messages.
- Calculation of distance error (x) [mm]
- Mean (\bar{x}) of distance error in x and y coordinate axes [mm]
- Standard deviation (σ) of distance error in x and y coordinate axes [mm]
- Relative standard deviation (RSD) of distance error in x and y coordinate axes [%]
- Variance (σ^2) of distance error in x and y coordinate axes [mm]

Calculation example for an examined slides is presented in Table 7. Meanwhile, the aggregated statistical evaluation based on all the examined slides is introduced in Table 8. The maximum achievable accuracy of the transformation with the given hardware and software components is approximately $2 \mu\text{m}$ in the x coordinate axis and $3 \mu\text{m}$ in the y coordinate axis, shown in the last row of Table 8.

Table 7
M_1__with_cross_cut_ref__40x slide ROI transformation evaluation

ROI number	distance [um]	target position x [mm]	target position y [mm]	transferred position x [mm]	transferred position y [mm]	distance error x [mm]	distance error y [mm]
1	1.2	42.812	12.572	42.811	12.573	0.001	0.001
2	1.2	43.090	12.749	43.089	12.751	0.001	0.002
3	2.8	45.279	12.443	45.277	12.446	0.002	0.003
4	0.0	46.137	13.338	46.137	13.338	0.000	0.000
5	2.9	50.650	11.862	50.648	11.868	0.002	0.006
6	3.7	62.172	16.296	62.170	16.296	0.002	0.000
7	2.9	64.761	16.858	64.759	16.859	0.002	0.001
8	1.2	62.005	14.711	62.004	14.715	0.001	0.004
9	1.6	63.993	15.064	63.992	15.065	0.001	0.001
10	0.0	60.402	13.868	60.402	13.868	0.000	0.000
11	0.0	64.880	14.692	64.880	14.692	0.000	0.000
12	2.3	61.341	13.789	61.339	13.789	0.002	0.000
13	4.1	64.932	14.053	64.930	14.056	0.002	0.003
14	3.6	63.087	12.125	63.086	12.130	0.001	0.005
15	2.9	65.594	11.714	65.595	11.718	0.001	0.004
16	4.0	65.308	7.458	65.306	7.466	0.002	0.008
17	3.2	63.790	9.079	63.788	9.085	0.002	0.006
18	5.8	68.610	12.279	68.611	12.284	0.001	0.005
average x [mm]	average y [mm]	standard deviation x [mm]	standard deviation y [mm]	relative standard deviation x [%]	relative standard deviation y [%]	variance x [mm]	variance y [mm]
0.0012777778	0.0027222222	0.0007519039	0.0025392346	59%	93%	0.0000005654	0.0000064477

Table 8
Aggregated statistical evaluation of the examined slides

Slide ID	Number of reference points	Number of measured ROIs	average x [um]	average y [um]	standard deviation x [um]	standard deviation y [um]	relative standard deviation x [%]	relative standard deviation y [%]	variance x [um]	variance y [um]
26	3	13	1.6154	0.3846	1.3868	0.5064	85.8%	131.7%	0.0019	0.0003
27	3	12	7.9167	3.0000	5.2994	4.0227	66.9%	134.1%	0.0281	0.0162
28	3	13	1.1538	1.0000	1.5730	1.4720	136.3%	147.2%	0.0025	0.0022
29	3	12	4.7500	2.0833	7.3870	2.7784	155.5%	133.4%	0.0546	0.0077
30	3	12	0.5833	0.5833	1.1645	0.9962	199.6%	170.8%	0.0014	0.0010
31	3	12	1.7500	5.3333	1.4848	2.8391	84.8%	53.2%	0.0022	0.0081
32	3	12	2.0000	1.5000	3.0451	2.0671	152.3%	137.8%	0.0093	0.0043
33	3	13	0.0055	7.0769	4.7717	4.5178	87.4%	63.8%	0.0228	0.0204
34	3	18	1.2778	2.7222	0.7519	2.5392	58.8%	93.3%	0.0006	0.0064
35	3	16	0.5625	0.3125	1.5478	1.0145	275.2%	324.6%	0.0024	0.0010
36	4	150	0.5479	1.7740	0.8144	2.2797	148.6%	128.5%	0.0007	0.0052
Total	34	283	1.7413	2.3687	2.1839	2.2255	129.6%	138.5%	0.0072	0.0065

It also points out that it is reasonable to work with a margin to ensure that the selected cell is cut out. Since the difference can vary in both positive and negative directions from the average, it is worth calculating twice the $2.22 \mu\text{m}$ standard deviation for the amount of margin. This means that at least $8\text{-}9 \mu\text{m}$ wide ROIs - that are 3 cell clusters - should be selected for post-laser dissection based on a pre-acquired static image for the equipment used.

Conclusions

In this paper, a software solution for automatic laser micro-dissection was developed for pathology purposes. It was found that the 3DHitech-P1000 digital tissue scanner and the MMI CellCut laser microdissector can be digitally linked. Without the use of resource-intensive image processing, it is only possible to perform a laser microdissection with μm accuracy based on a static image taken in advance by placing at least three reference points. The new workflow limitations are preparational, scanner, dissector, and also transformation technical constraints that determine the overall accuracy. The total accuracy is about $8\text{-}9 \mu\text{m}$ which means there should 3 cell clusters be selected for post-laser dissection based on a pre-acquired static image for the equipment used.

Furthermore, for the microdissector to be able to check automatically whether the inserted slide and the imported xml file are in pair instead of the user mentioned in 2.4.3, it would be necessary to take a preview image of the label of the inserted tissue sample, read the sample ID, and compare it with the name of the imported xml file. Implementing this would require hardware-level changes to the equipment. So it is not feasible with the current LMC equipment at the moment, but could be a new direction of development in the future.

In the next development phase, a huge emphasis could also be put on software development on genomics pattern detection, then the fusion of genomics and morphology at data storage, joint evaluation, and visualization.

Acknowledgment

The authors would like to thank the Applied Informatics and Applied Mathematics Doctoral School of Óbuda University, Budapest, Hungary for their support in this research.

References

- [1] K. Schütze *et al.* Identification of expressed genes by laser-mediated manipulation of single cells. *Nat Biotechnol*, 16(7):737–742, 1998.
- [2] F. Tang *et al.* Whole transcriptome amplification: Methods and pitfalls. *Current Opinion in Biotechnology*, 2009.
- [3] M. Schena *et al.* Tissue microdissection coupled with rna amplification and its use in the exploration of mars. *Research in Microbiology*, 1995.
- [4] R. Prado *et al.* High-quality rna extraction from polyethylene glycol-precipitated polysaccharides in polysaccharide-rich marine macroalgae. *Plant Molecular Biology Reporter*, 2014.
- [5] T. Bhamidipati *et al.* Laser capture microdissection in the spatial analysis of epigenetic modifications in skin: A comprehensive review. *Oxidative Medicine and Cellular Longevity*, 2022(4127238):12, 02 2022.
- [6] I. A. Eltoun *et al.* Microdissection of histologic sections: Past, present, and future. *Advances in Anatomic Pathology*, 9(5):316–322, 2002.
- [7] R. Jiang *et al.* A review on laser microdissection technologies. *Bioengineered*, 2013.
- [8] A. Rabien *et al.* Tissue microdissection. *Methods Mol Biol*, (1381):39–52, 2016.
- [9] B. Alberts *et al.* Molecular biology of the cell. 4th edition. *Garland Science*, 2002.
- [10] M. Emmert-Buck *et al.* Laser capture microdissection: Molecular analysis of tissue. *Science*, 274(5289):998–1001, 1996.
- [11] R. Bonner *et al.* Laser capture microdissection: Methods and applications. *Molecular Pathology*, 1997.
- [12] F. Monzon *et al.* Laser capture microdissection: Arcturus(xena) veritas laser capture microdissection system. *BioTechniques*, 2009.
- [13] Molecular Machines & Industries. Single cell picking like a pro: MMI CellEctor. <https://www.molecular-machines.com/products/cell-picker>. Accessed: 2023-12-08.
- [14] Leica Microsystems. Leica LMD6500 LMD7000 Laser Microdissection Systems. <https://www.leica-microsystems.com/products/light-microscopes/p/leica-lmd7000/>. Accessed: 2024-06-10.
- [15] Sackler Interdepmental Core Facility of Tel Aviv University. ArcturusXT™ Laser Capture Microdissection (LCM) System. <https://sicf.tau.ac.il/scmic/lcm-arcturus/>, 2020. Accessed: 2024-06-10.
- [16] University of Delaware. CryoJane® User Manual. <https://bioimaging.dbi.udel.edu/wp-content/uploads/2015/12/CryoJaneUserMan.pdf>, 2015. Accessed: 2024-06-10.

- [17] Leica Biosystems. Leica CM3050 S Cryostat. <https://www.leicabiosystems.com/histology-equipment/cryostats/leica-cm3050-s/>. Accessed: 2024-06-10.
- [18] Medtronic. Electrosurgical Hardware, Valleylab™ FT10 Energy Platform. <https://www.medtronic.com/covidien/en-us/products/electrosurgical-hardware/valleylab-ft10-energy-platform.html>. Accessed: 2024-06-10.
- [19] Olympus America. Thunderbeat. <https://medical.olympusamerica.com/products/thunderbeat>, 2024. Accessed: 2024-06-10.
- [20] Scientific Laboratory Supplies Ltd. ROCHE Liberase TM Research Grade 100 Mg. <https://www.scientificlabs.co.uk/product/pcr-kits-and-reagents/5401127001>. Accessed: 2024-06-10.
- [21] Sakura USA. Tissue-Tek® Cryo3® Flex Cryostat. <https://www.sakuraus.com/Products/Cryotomy/Tissue-Tek-Cryo3-Flex-Cryostat.html>. Accessed: 2024-06-10.
- [22] Leica Microsystems. Ultramicrotomes & Cryo-Ultramicrotomes. <https://www.leica-microsystems.com/products/sample-preparation-for-electron-microscopy/ultramicrotomes-cryo-ultramicrotomes/>. Accessed: 2024-06-10.
- [23] B. Aguilar-Bravo *et al.* Laser capture microdissection: techniques and applications in liver diseases. *Hepatology International*, (13):138–147, 2019.
- [24] R. B. Priya *et al.* Role of industry 4.0 technologies in enhancing sustainable firm performance and green practices. *Acta Polytechnica Hungarica*, 19(8):229–248, 2022.
- [25] M. D. Kucarov *et al.* Single cell position determination and transformation from static high-resolution digital image to laser-microdissector coordinate system using image processing techniques. *IEEE 17th International Symposium on Applied Computational Intelligence and Informatics (SACI)*, pages 195–202, 05 2023.
- [26] 3DHISTECH. Panoramic 1000 user’s guide. <https://assets.thermofisher.com/TFS-Assets/APD/Product-Guides/US-Only-P1000-BF-Users-Guide-EN-2018-04.pdf>, 2018. Accessed:2023-12-08.
- [27] M. Kozlovsky *et al.* Parameter assisted HE colored tissue image classification. *IEEE 17th International Conference on Intelligent Engineering Systems (INES)*, 10 2013.
- [28] M. D. Kucarov *et al.* Using geospatial-aimed ecognition in biomedical field for gland detection. *IEEE 21st World Symposium on Applied Machine Intelligence and Informatics (SAMI)*, pages 307–313, 01 2023.
- [29] M. D. Kucarov *et al.* Patho-genomics fused database schema and optimization for automatic pathology workflow. *IEEE 21st World Symposium on Applied Machine Intelligence and Informatics (SAMI)*, pages 317–324, 01 2023.
- [30] Molecular Machines & Industries GmbH. mmi CellCut User Manual. <https://ethz.ch/content/dam/ethz/special-interest/dual/scope/instruments/Manuals/mmiCellCut-manual%205.1.pdf>, 2020. Accessed:2023-12-08.

Attachments

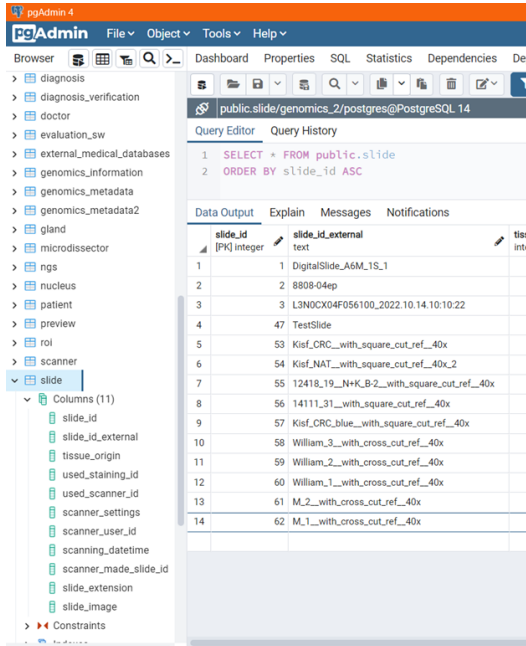


Figure 9

Part of the uploaded slides in SLIDE table

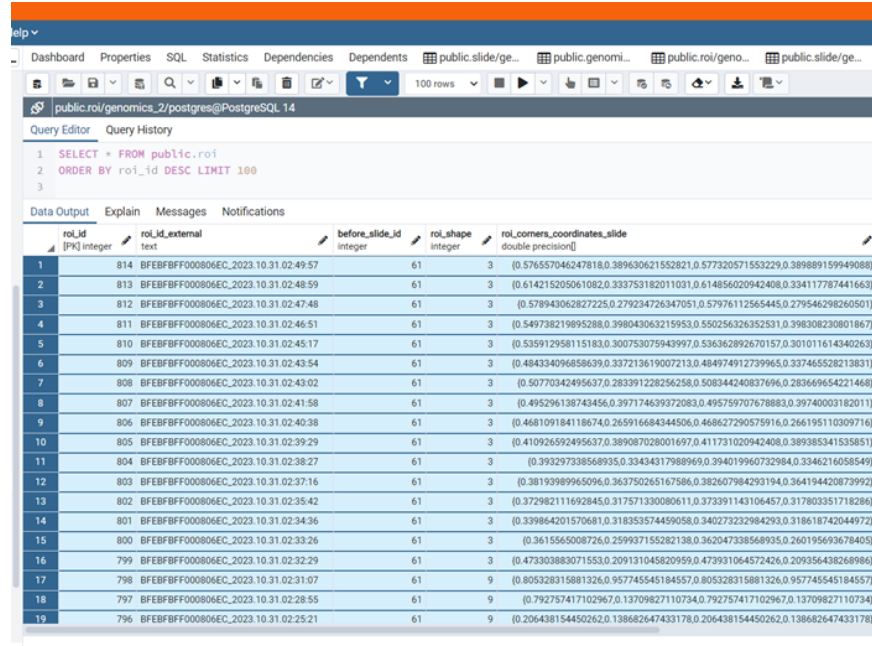


Figure 10

Part of the selected ROIs in ROI table

```
G:\munka\Obudai_Egyetem\2_LMD_project\nyar\3_development\6_XML\Slide_ROK_2023.09.15_10_48_36-CaJ_CRC_16um_40x.xml - Notepad++
File Edit Search View Encoding Language Settings Tools Macro Run Plugins Window ?
Slide_ROK_2023.09.15_10_48_36-CaJ_CRC_16um_40x.xml
1 <?xml version="1.0" encoding="utf-8"?>
2 <GroupsAndShapes xmlns="http://molecular-machines.com">
3   <StageInserts BoundingBoxLeft="-22.1" BoundingBoxRight="137.9" BoundingBoxTop="-13.4" BoundingBoxBottom="96.6" Geometry="0" Info="" Name="" NumberOfSlides="3" />
4   <Slide BoundingBoxLeft="26" BoundingBoxRight="102" BoundingBoxTop="-1.5999999999999999" BoundingBoxBottom="24.4" Geometry="0" Info="" Name="A1" />
5   <Slide BoundingBoxLeft="25.9" BoundingBoxRight="101.9" BoundingBoxTop="27.2" BoundingBoxBottom="53.2" Geometry="0" Info="" Name="B1" />
6   <Slide BoundingBoxLeft="25.7" BoundingBoxRight="101.7" BoundingBoxTop="55.6" BoundingBoxBottom="81.6" Geometry="0" Info="" Name="C1" />
7   <Group Name="OutAndCollect" CoordinateSystem="1" Visible="1" Listed="1" MultiSelect="1" Cutable="1" Collectable="1" ShowLabel="1" ShowShapeCenter="0" TagIndex="1" PenColor="65280" PenWidth="1"
8     MaxNumShapes="0">
9     <Shape Type="3" Cut="0" Outable="1" Collected="0" Collectable="1" Microscope2="-999999999" Closed="1" Use="0" CellsParent="A1" BoundingBoxLeft="39.871764705882342" BoundingBoxRight="
10      39.988235294117636" BoundingBoxTop="15.026144444444444" BoundingBoxBottom="15.134800000000002" Geometry="0" Info="" Name="BFZBFBFF000806EC_2023.09.15.10:50:45">
11       <Point X="39.871764705882342" Y="15.026144444444444" />
12       <Point X="39.988235294117636" Y="15.134800000000002" />
13     </Shape>
14     <Shape Type="2" Cut="0" Outable="1" Collected="0" Collectable="1" Microscope2="-999999999" Closed="1" Use="0" CellsParent="A1" BoundingBoxLeft="41.238352941176451" BoundingBoxRight="
15      41.370352941176456" BoundingBoxTop="14.071527777777774" BoundingBoxBottom="14.110333333333326" Geometry="0" Info="" Name="BFZBFBFF000806EC_2023.09.15.10:51:29">
16       <Point X="41.238352941176451" Y="14.110333333333326" />
17       <Point X="41.370352941176456" Y="14.071527777777774" />
18     </Shape>
19     <Shape Type="1" Cut="0" Outable="1" Collected="0" Collectable="1" Microscope2="-999999999" Closed="1" Use="0" CellsParent="A1" BoundingBoxLeft="41.711999999999982" BoundingBoxRight="
20      41.843999999999987" BoundingBoxTop="15.584944444444439" BoundingBoxBottom="15.716883333333326" Geometry="0" Info="" Name="BFZBFBFF000806EC_2023.09.15.10:52:03">
21       <Point X="41.711999999999982" Y="15.650913888888887" />
22       <Point X="41.843999999999987" Y="15.650913888888887" />
23     </Shape>
24     <Shape Type="4" Cut="0" Outable="1" Collected="0" Collectable="1" Microscope2="-999999999" Closed="1" Use="0" CellsParent="A1" BoundingBoxLeft="42.558352941176452" BoundingBoxRight="
25      42.667058823529395" BoundingBoxTop="17.765816666666662" BoundingBoxBottom="17.959844444444435" Geometry="0" Info="" Name="BFZBFBFF000806EC_2023.09.15.10:52:21">
26       <Point X="42.558352941176452" Y="17.862830555555547" />
27       <Point X="42.667058823529395" Y="17.862830555555547" />
28     </Shape>
29     <Point X="42.612705882352927" Y="17.959844444444435" />
30   </Group>
31   <Group Name="REFERENCE" CoordinateSystem="1" Visible="1" Listed="0" MultiSelect="0" Cutable="0" Collectable="0" ShowLabel="1" ShowShapeCenter="1" TagIndex="1" PenColor="15673865" PenWidth="1"
32     MaxNumShapes="3">
33     <Shape Type="9" Cut="0" Outable="1" Collected="0" Collectable="1" Microscope2="-999999999" Closed="1" Use="0" CellsParent="A1" BoundingBoxLeft="33" BoundingBoxRight="33" BoundingBoxTop="
34      3.400000000000001" BoundingBoxBottom="3.400000000000001" Geometry="0" Info="" Name="">
35       <Point X="33" Y="3.400000000000001" />
36     </Shape>
37     <Shape Type="9" Cut="0" Outable="1" Collected="0" Collectable="1" Microscope2="-999999999" Closed="1" Use="0" CellsParent="A1" BoundingBoxLeft="32.9844705882353" BoundingBoxRight="32.9844705882353"
38       BoundingBoxTop="19.457738888888893" BoundingBoxBottom="19.457738888888893" Geometry="0" Info="" Name="">
39       <Point X="32.9844705882353" Y="19.457738888888893" />
40     </Shape>
41     <Shape Type="9" Cut="0" Outable="1" Collected="0" Collectable="1" Microscope2="-999999999" Closed="1" Use="0" CellsParent="A1" BoundingBoxLeft="77.957647058823454" BoundingBoxRight="
42       77.957647058823454" BoundingBoxTop="19.550872222222218" BoundingBoxBottom="19.550872222222218" Geometry="0" Info="" Name="">
43       <Point X="77.957647058823454" Y="19.550872222222218" />
44     </Shape>
45   </Group>
46 </GroupsAndShapes>
```

Figure 11
Exported XML file sample from MorphCheck